JMEPEG (2012) 21:1509–1513
DOI: 10.1007/s11665-011-0049-3

1059-9495/$19.00

# PMMA/$Zn_2SiO_4$:$Eu^{3+}$($Mn^{2+}$) Composites: Preparation, Optical, and Thermal Properties

*Ljubica Đačanin, Svetlana R. Lukić, Dragoslav M. Petrović, Željka Antić, Radenka Krsmanović, Milena Marinović-Cincović, and Miroslav D. Dramićanin*

*(Submitted January 5, 2011; in revised form July 31, 2011)*

**Luminescent composites of poly(methylmethacrylate) (PMMA) and nanophosphors ($Zn_2SiO_4$:$Mn^{2+}$, $Zn_2SiO_4$:$Eu^{3+}$) were prepared by dispersion casting method. It was found that nanoparticles embedded in PMMA matrix preserve their typical phosphorescence emission. The influence of $Zn_2SiO_4$ nanofillers on thermal properties of PMMA was also investigated. A shift towards higher glass transition temperatures and slight improvements in thermal stability of the nanocomposites compared to pure PMMA were observed and are discussed herein.**

**Keywords** advanced characterization, material selection, polymer matrix composites

## 1. Introduction

In recent years, there has been an increased interest in obtaining and investigating composites consisting of nanoparticles and polymer materials. There are many reasons for this; such composites retain unique size-dependent properties, while favorable characteristics of the polymer material are also preserved. In addition, novel and significantly enhanced physical and chemical properties, along with biological functions, phenomena, and processes often emerge due to synergetic effects. The properties of polymer nanocomposites depend on the type of nanoparticles that are incorporated, the size and shape of the particles, and the concentration and interaction with the polymer matrix.

Phosphor nanoparticles, i.e., nanophosphors, are of special interest due to many important applications, ranging from solid-state lightning and displays to biomedicine. Zinc silicate ($Zn_2SiO_4$) has been identified as a suitable host matrix for many transition metal and rare earth (RE) dopant ions, providing excellent luminescent properties in the blue, green, and red spectral zones (Ref 1). Manganese-doped zinc silicate, $Zn_2SiO_4$:$Mn^{2+}$, has been used extensively as a green luminescent phosphor in cathode ray tubes, lamps, and plasma display panels for a number of reasons, including its high saturated color, strong luminescence, long life span, lack of moisture sensitivity, and chemical stability (Ref 1–7). On the other hand, doping with RE ions having special 4f intra-shell transitions and narrow characteristic emission bands yield brightly colored luminescent materials (Ref 8).

Among the wide variety of available polymers, poly(methylmethacrylate) (PMMA) represents a particularly suitable matrix for embedding functional, nanoscopic inorganic fillers due to its outstanding mechanical, chemical, and physical properties. PMMA has seen widespread application in many technological fields that exploit the unique combination of excellent optical properties (clarity, transparency from the near UV to the near IR), chemical inertness, good mechanical and electrical properties, thermal stability, weather resistance, formability, and moldability (Ref 9). Further advantages of using PMMA lie in its extensive availability and easy preparation (Ref 10). PMMA embedded with inorganic or organically modified inorganic particles have been cast into films, yielding enhanced photoconductivity (Ref 11), photoinduced charge-transfer (Ref 12), nonlinear optical properties (Ref 13), photoluminescence (Ref 14, 15), along with various mechanical (Ref 16), thermal (Ref 17–19), and magnetic properties (Ref 20).

In this paper, we analyze the luminescence and thermal properties of PMMA/nanophosphors ($Zn_2SiO_4$:$Mn^{2+}$, $Zn_2SiO_4$:$Eu^{3+}$) composites obtained via dispersion casting method from presynthesized phosphor nanopowders. These composite types have potential applications in toy-making industries and various uses in lightning for the illumination of safety signs and many others. Recently, Miyazaki et al. investigated PMMA/$Zn_2SiO_4$:$Mn^{2+}$ composites, and their results confirm good storage stability and screen printability (Ref 21).

## 2. Experimental

First, nanopowders of $Zn_2SiO_4$ doped with 3 at.% of $Mn^{2+}$ and 1 at.% of $Eu^{3+}$ were synthesized. Nanocrystalline powders were obtained using a previously published polymer-assisted sol-gel method (Ref 21). Starting materials included tetraethyl orthosilicate (TEOS) (Aldrich, 98%), zinc oxide (Alfa Aesar, p.a.), manganese nitrate (Aldrich, p.a.), and europium oxide (Aldrich, p.a), with ethanol as the solvent. Polyethylene glycol with an average molecular weight of 200 (PEG 200, Alfa

**Ljubica Đačanin, Svetlana R. Lukić,** and **Dragoslav M. Petrović**, Department of Physics, University of Novi Sad, 21000 Novi Sad, Serbia; and **Željka Antić, Radenka Krsmanović, Milena Marinović-Cincović,** and **Miroslav D. Dramićanin**, Vinča Institute of Nuclear Sciences, University of Belgrade, P.O. Box 522, 11001 Belgrade, Serbia. Contact e-mail: zeljkaa@gmail.com.

Aesar) was used as fuel for the combustion reaction. For the synthesis of the $Zn_2SiO_4:Mn^{2+}$ nanophosphor, aqueous solutions containing appropriate concentrations of zinc and manganese nitrate were prepared by dissolving zinc oxide in 6 M nitric acid and an adequate quantity of manganese nitrate in water. An ethanol solution containing an equimolar amount of TEOS was added to the aqueous mixture. Next, PEG 200 was added to the resulting sol in a 1:1 mass ratio to the expected mass of the final product, and the mixture was stirred for 60 min at room temperature. The acidity was adjusted by slowly adding ammonia solution and stirring until a gel was derived. After drying at 100 °C for 5 days, the dry gel was fired in a microwave oven (800 W for 5 min) and then thermally treated in a furnace at 1180 °C for 1 h. The same procedure with europium oxide as the dopant precursor was used to obtain the $Zn_2SiO_4:Eu^{3+}$ nanophosphor.

Nanocomposites of PMMA/$Zn_2SiO_4:Mn^{2+}$ and PMMA/$Zn_2SiO_4:Eu^{3+}$ were prepared by dispersing an appropriate amount of nanophosphors in a xylene solution of commercially available Diakon CMG 314V PMMA ($M_w$ = 90,000; $M_w/M_n$ = 2.195). Initially, the nanopowders were dispersed in xylene (Aldrich) by stirring at a high sheer rate for 18 h, followed by treatment in an ultrasonic bath for 3 h. The PMMA was dissolved in the same amount of xylene. Next, the slurry of phosphor nanoparticles was added to the polymer solution, and the mixture was poured over a flat surface. After evaporation of the solvent under ambient conditions, the content of nanophosphors in PMMA matrices was 3 mass%.

X-ray diffraction measurements of pure and doped PMMA composites were obtained with a Philips PW 1050 instrument using Ni-filtered Cu Kα 1,2 radiation. Diffraction data were recorded in a 2θ range from 5° to 80° counting for 10 s in 0.02° steps.

Photoluminescence emission spectra and lifetime measurements were performed at room temperature on the Fluorolog-3 Model FL3-221 spectroflurometer system (HORIBA Jobin-Yvon), incorporating a 450 W Xenon lamp for emission measurements and a 150 W pulsed Xenon lamp for lifetime measurements, while a TBX detector was utilized in both cases.

The thermal stability of pure PMMA and PMMA/$Zn_2SiO_4$ samples was investigated using non-isothermal thermo-gravimetric analysis (TG) and differential thermal analysis (DTA) with a SETARAM SETSYS Evolution-1750 instrument. These measurements were conducted at a heating rate of 10 °C/min in a dynamic argon atmosphere (flow rate 20 $cm^3$/min) over a temperature range of 30 to 500 °C.

Differential scanning calorimetry (DSC) measurements of pure PMMA and PMMA/$Zn_2SiO_4$ samples were performed on a Perkin-Elmer DSC-2 instrument over a temperature range of 50 to 150 °C, with a heating rate of 20 °C/min. In an effort to prepare samples with the same thermal history, samples were heated prior to measurements above the glass transition temperature and then cooled down (heating and cooling rates were 20 °C/min).

The basic properties of zinc silicate particles used for the preparation of composites have been previously presented in detail (Ref 22, 23).

## 3. Results and discussion

XRD diffractograms obtained from pure PMMA and PMMA/$Zn_2SiO_4:Mn^{2+}$ ($Eu^{3+}$) composites are presented in Fig. 1. Complete matching of composites diffraction peaks and the agreement with the JCPDS No. 37-1485 card data of $Zn_2SiO_4$ can be seen. The broad region at low angles can be attributed to amorphous PMMA. A slight shift of composites diffraction peaks is a consequence of the differences in the ionic radius of europium and manganese ions.

In the investigated composites, luminescence emission is obtained via electronic transitions in $Eu^{3+}$ and $Mn^{2+}$ dopant ions. Such emissions are characteristic of these ions and are influenced by chemical surroundings. Under ordinary conditions, $Zn_2SiO_4$ crystallizes in phenacite structural type and belongs to the rhombohedral space group $R\bar{3}$ (No. 148), where all ions occupy general crystallographic positions [$x$, $y$, $z$] (18f in hexagonal axis set or 6f in rhombohedral axis set) with local symmetry 1. Because all of the ions are in crystallographic positions of the same type, to comply with stoichiometry, the zinc ions will occupy two crystallographic positions, the silicon ions one position, and the oxygen ions will occupy four different 18f (6f) crystallographic positions. In both non-equivalent crystallographic positions, zinc ions are tetrahedrally coordinated with oxygen ions. This is important for understanding the luminescence of $Zn_2SiO_4:Eu^{3+}$ and $Zn_2SiO_4:Mn^{2+}$, as europium and manganese ions substitute zinc in this structure. These two tetrahedrons are almost regular, are very similar and provide almost identical surrounding for dopant ions.

Our previous work has investigated the luminescence properties of manganese-doped (Ref 22) and europium-doped (Ref 23) $Zn_2SiO_4$ powders. Emission spectra of a PMMA/$Zn_2SiO_4:Eu^{3+}$ composite is presented in Fig. 2. Emissions associated to $^5D_0 \rightarrow {}^7F_i$ ($i$ = 0, 1, 2, 3, and 4) spin forbidden f-f transitions are observed. At 579.2 nm, an emission from $^5D_0 \rightarrow {}^7F_0$ transition can be seen. The $^5D_0 \rightarrow {}^7F_1$ transition is the parity-allowed magnetic dipole transition ($\Delta J$ = 1), and its intensity is not influenced by the host. For this transition, three distinct emission lines situated at 589.2, 592.6, and 597.1 nm are present ($2J + 1 = 3$), with the energy of crystal field splitting $\Delta E$ = 224.5 $cm^{-1}$. The $^5D_0 \rightarrow {}^7F_2$ electric dipole transition ($\Delta J = 2$) is very sensitive to the local environment around $Eu^{3+}$ ions, and its intensity depends on the symmetry of the crystal field. The emission from this transition is the most intense and is positioned at 612 nm. A low symmetry around RE cations increases the emission strength of the electric dipole transition. In this sense, it is

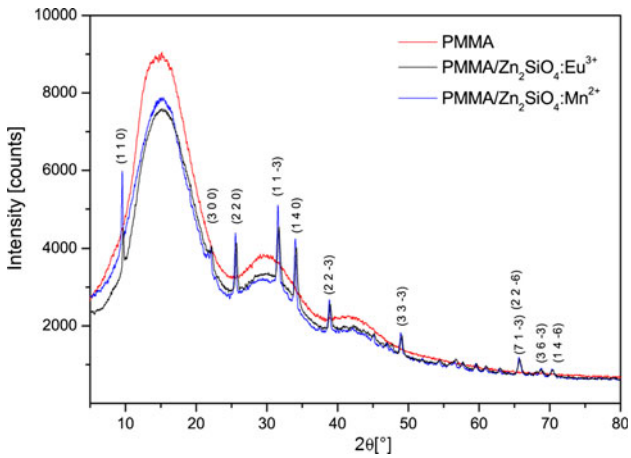


**Fig. 1** XRD spectra of pure PMMA and PMMA/$Zn_2SiO_4:Mn^{2+}$ ($Eu^{3+}$) composites

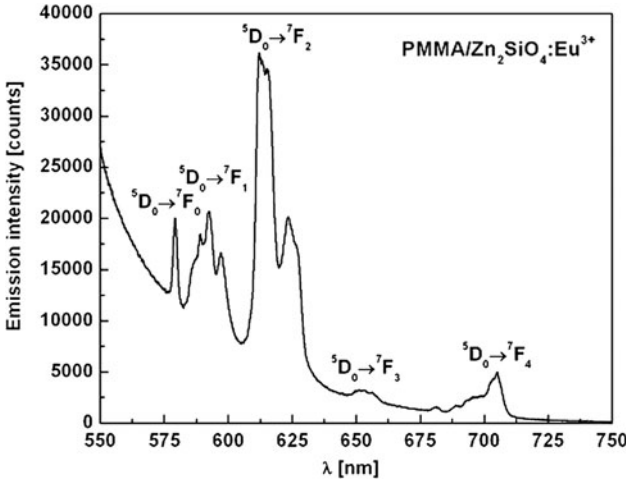


**Fig. 2** Emission spectra of PMMA/$Zn_2SiO_4$:$Eu^{3+}$ composite after excitation at 393 nm

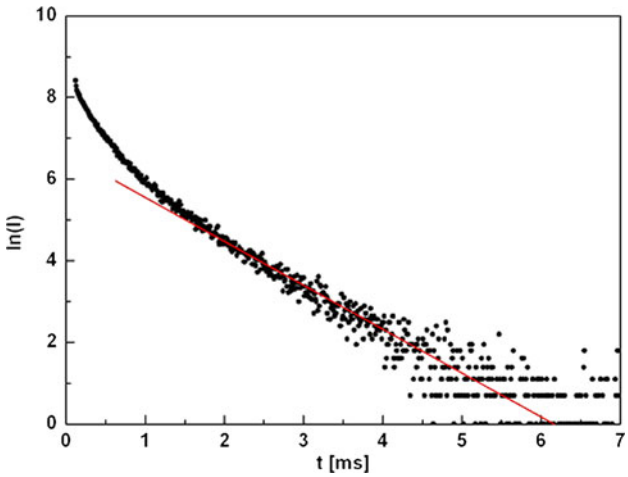


**Fig. 3** Luminescence decay profile at room temperature of the PMMA/$Zn_2SiO_4$:$Eu^{3+}$ composite measured at 612 nm after excitation at 393 nm. Lifetime is estimated to be 0.93 ms

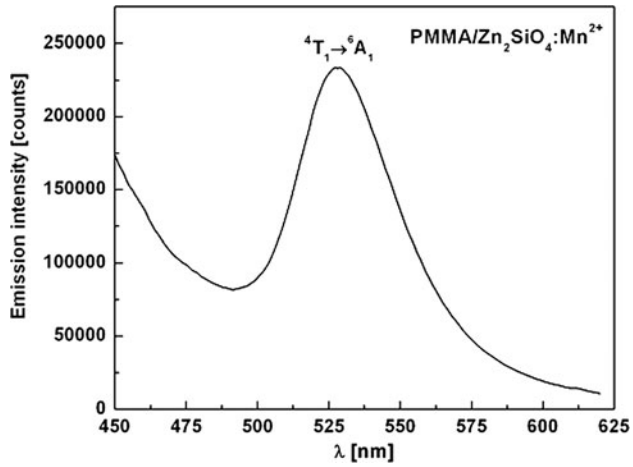


**Fig. 4** Emission spectra of PMMA/$Zn_2SiO_4$:$Mn^{2+}$ composite after excitation at 356 nm

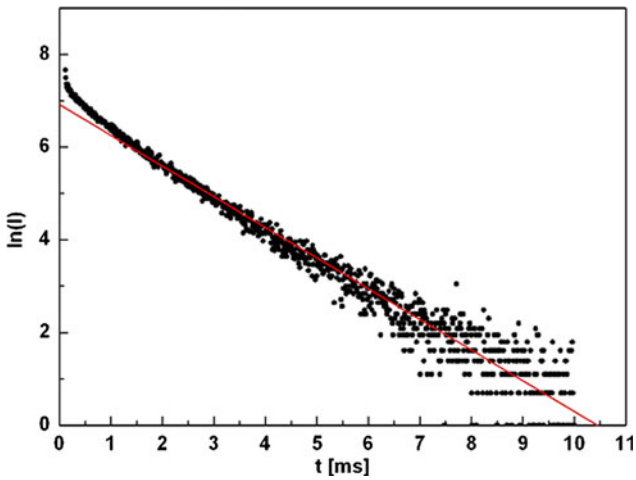


**Fig. 5** Luminescence decay profile at room temperature of the PMMA/$Zn_2SiO_4$:$Mn^{2+}$ composite measured at 526 nm after excitation at 356 nm. Lifetime is estimated to be 1.51 ms

generally acknowledged that the ratio of the emission intensities $R = \frac{I(^5D_0 \rightarrow ^7F_2)}{I(^5D_0 \rightarrow ^7F_1)}$ is an asymmetry parameter for the $Eu^{3+}$ sites and a measure of the extent of its interaction with surrounding ligands. The asymmetry parameter was calculated from the peak intensities to be 1.75. Emissions from $^5D_0 \rightarrow {}^7F_3$ and $^5D_0 \rightarrow {}^7F_4$ transitions can be seen at 653 and 705 nm, respectively. From this data and the support of previously published works (Ref 22, 23), one may conclude that the optical emission, the main function of inorganic phosphor fillers, is completely preserved in the prepared composites.

The results of the emission lifetime measurements for the PMMA/$Zn_2SiO_4$:$Eu^{3+}$ composite are presented in Fig. 3. The luminescence decay profile could be adjusted by a single-exponential function for the longer time range, while a non-exponential part is observed for the short times. The estimated lifetime of 0.93 ms is a rather high value characteristic for europium species with low non-radiative energy transfer probability. This value is slightly higher compared to 0.8 ms, measured for $Zn_2SiO_4$:$Eu^{3+}$ (Ref 23).

The emission spectra of the PMMA/$Zn_2SiO_4$:$Mn^{2+}$ composite is presented in Fig. 4. In tetrahedral coordination (weak crystal field), $Mn^{2+}$ exhibits green luminescence from the $^4T_1(G) \rightarrow {}^6A_1(S)$ transition, peaking at 526 nm. It should be noted that the emission spectrum does not have a simple Gaussian shape due to some coordinate displacement of the potential energy curves. A tailing in the long wavelength portion of the emission band is visible in Fig. 4 (Ref 24). From emission decay data, presented in Fig. 5, the emission lifetime is estimated to 1.5 ms. This value is slightly lower compared to 1.6 ms, measured for pure $Zn_2SiO_4$:$Mn^{2+}$ (Ref 22).

The glass transition behavior of the PMMA and nanocomposites was investigated using DSC. The heat capacity curves of the pure PMMA and PMMA/ $Zn_2SiO_4$ nanocomposites are shown in Fig. 6. After incorporation of $Zn_2SiO_4$ into the PMMA matrix, a shift in the slope of the heat capacity curves towards higher temperatures was observed. This slope corresponds to the glass transition temperature ($T_g$) of the polymer. It should be emphasized that the glass transition is not a true phase transition because the derivative of the heat capacity can

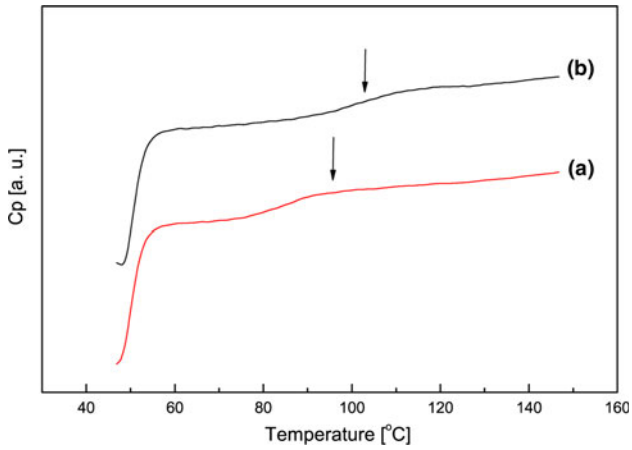


**Fig. 6** The heat capacity curves of the (a) pure PMMA and (b) PMMA/$Zn_2SiO_4$ nanocomposites

**Table 1 Glass transition temperature and temperatures of peak position of DTA curves of PMMA and PMMA/$Zn_2SiO_4$ obtained in argon atmosphere**

| Sample | $T_g$, °C | $T_{max\ 1}$, °C | $T_{max\ 2}$, °C |
|---|---|---|---|
| Pure PMMA | 96 | 293 | 375 |
| PMMA/$Zn_2SiO_4$ | 103 | 299 | 384 |

be a continuous function of temperature. The different segmental motions lead to the glass transition spectrum.

The values of the glass transition temperature were taken as the midpoint of the glass event. The values obtained for PMMA and PMMA/$Zn_2SiO_4$ nanocomposites are listed in Table 1.

It can be seen from Table 1 that the glass transition temperatures of the PMMA/$Zn_2SiO_4$ (103 °C) are higher than that of pure PMMA (96 °C).

This effect can be explained as a consequence of decreased molecular mobility of the PMMA chains due to adhesion of polymer segments onto the surface of $Zn_2SiO_4$ particles. For this reason, the glass transition temperature of PMMA/$Zn_2SiO_4$ is higher than for pure PMMA.

The broadening of the glass transition region for the PMMA/$Zn_2SiO_4$ was also observed. If it is assumed that the $T_g$ corresponds to the motion of segments with some average length, then the presence of filler particles will alter the distribution of segmental lengths and consequently induce changes in the glass transition region.

The thermal stability of PMMA and PMMA/$Zn_2SiO_4$ samples was examined using non-isothermal thermo-gravimetry. TG curves obtained for pure PMMA and PMMA/$Zn_2SiO_4$ samples in an argon atmosphere are shown in Fig. 7. It is known that PMMA thermally decomposes by depolymerization (Ref 25). The thermal stability of free radically polymerized PMMA is significantly affected by the presence of unsaturated end groups and head-to-head bonds obtained during termination by disproportionation and combination, respectively. The thermal degradation of PMMA usually occurs in three stages, characterized by three maxima in the DTA curve at about 180, 300, and 380 °C at a heating rate of 10 °C/min (Ref 26–29). These stages have been attributed to different modes of initiation of depolymerization. The first peak corresponds to depolymerization initiated by the scission of the weak head-to-head bonds

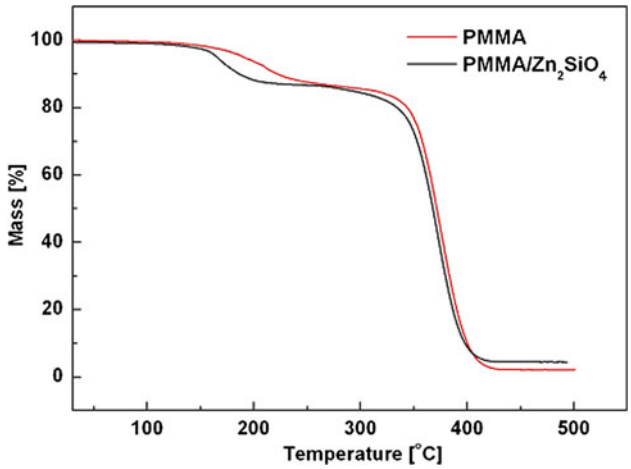


**Fig. 7** TG curves of pure PMMA and PMMA/$Zn_2SiO_4$ nanocomposites obtained in an argon atmosphere at a heating rate of 10 °C/min

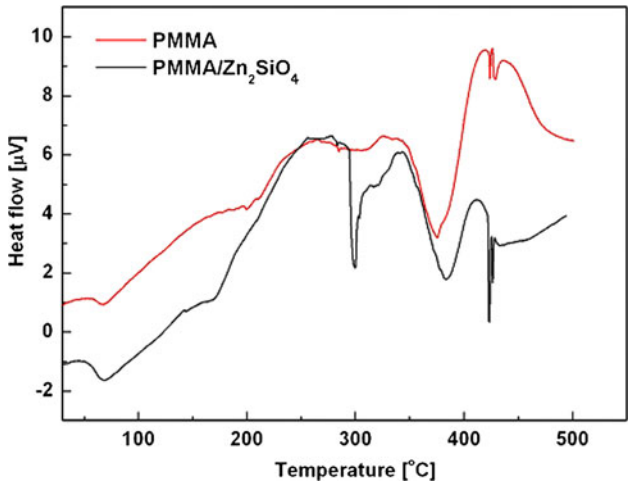


**Fig. 8** DTA curves of pure PMMA and PMMA/$Zn_2SiO_4$ nanocomposites obtained in an argon atmosphere at a heating rate of 10 °C/min

while the second stage corresponds to depolymerization initiated by the unsaturated vinyl chain ends. The third peak corresponds to depolymerization initiated by random main chain scission. The DTA curves of pure PMMA and PMMA/$Zn_2SiO_4$ samples are shown in Fig. 8. The thermal degradation of pure PMMA and PMMA/$Zn_2SiO_4$ samples in our experiment occurs in two stages, with the TG and DTA curves being very similar. The most intense DTA peak for both samples was at approximately 380 °C (374.6 °C for pure PMMA and 383 °C for PMMA/$Zn_2SiO_4$), corresponding to depolymerization initiated by random chain scission. The absence of the peak at 180 °C indicates the lack of head-to-head bonds in PMMA chains.

The obtained results indicate that after the incorporation of $Zn_2SiO_4$ powder, the thermal stability of the PMMA matrix is slightly improved.

## 4. Conclusions

In this paper, we have presented a simple method for the preparation of PMMA/nanophosphor ($Zn_2SiO_4:Eu^{3+}$, $Zn_2SiO_4:Mn^{2+}$)

composites. The materials obtained exhibited characteristic luminescence emissions from electronic transitions in trivalent europium and divalent manganese ions, red and green, respectively. The observed lifetime values, 0.93 ms for $Eu^{3+}$ ion and 1.51 ms for $Mn^{2+}$ ion composites, are quite high and suggest successful encapsulation of dopant ions in the polymer through the zinc silicate host. From this data one may conclude that optical emission, the main function of inorganic phosphor filler, is completely preserved in prepared composites. Additionally, thermal analyses produced evidence of slightly improved thermal stability and higher glass transition temperatures of the polymer phase in these composites. The materials obtained also display combined features of both composite components, inorganic and organic, and for this reason may have useful applications.

## Acknowledgments

The authors are grateful to Dr. Miodrag Mitrić for performing the XRD measurements. The authors acknowledge the support of the Ministry of Science of the Republic of Serbia (project numbers 141026 and 142066).

## References

1. X. Quyang, A.H. Kitai, and T. Xiao, Electroluminescence of the Oxide Thin Film Phosphors $Zn_2SiO_4$ and $Y_2SiO_5$, *J. Appl. Phys.*, 1996, **79**(6), p 3229–3234
2. A. Manavbasi and J.C. Lacombe, Synthesis of Pure $Zn_2SiO_4$:Mn Green Phosphors by Simple PVA-Metal Complex Route, *J. Mater. Sci.*, 2007, **42**(1), p 252–258
3. T.H. Cho and H.J. Chang, Preparation and Characterizations of $Zn_2SiO_4$:Mn Green Phosphors, *Ceram. Int.*, 2003, **29**(6), p 611–688
4. Y.C. Kang and H.D. Park, Brightness and Decay Time of $Zn_2SiO_4$:Mn Phosphor Particles with Spherical Shape and Fine Size, *Appl. Phys. A*, 2003, **77**(3–4), p 529–532
5. A. Morell and N.E. Khiati, Green Phosphors for Large Plasma TV Screens, *J. Electrochem. Soc.*, 1993, **140**(7), p 2019–2022
6. Y. Kotera, Luminescent Materials, *J. Jpn. Soc. Color Mater.*, 1985, **58**(2), p 80–88
7. J. Lin, D.U. Sänger, M. Mennig, and K. Bärner, Sol–Gel Synthesis and Characterization of $Zn_2SiO_4$:Mn Phosphor Films, *Mater. Sci. Eng. B*, 1999, **64**(2), p 73–78
8. S.M. Liu, F.Q. Liu, H.Q. Guo, Z.H. Zhang, and Z.G. Wang, Correlated Structural and Optical Investigation of Terbium-Doped Zinc Oxide Nanocrystals, *Phys. Lett. A*, 2000, **271**(1–2), p 128–133
9. H.F. Mark, N.M. Bikales, C.G. Overberger, and G. Menges, *Encyclopedia of Polymer Science and Technology*, 1st ed., John Wiley and Sons, New York, 1985
10. S. Gross, D. Camozzo, V. Di Noto, L. Armelao, and E. Tondello, PMMA: A Key Macromolecular Component for Dielectric Low-κ hybrid inorganic–organic polymer films, *Eur. Polym. J.*, 2007, **43**(3), p 673–696
11. A. Thander and B. Mallik, Observation of Persistent Photoconductivity at Room Temperature in Ferrocene-Doped Poly(methylmethacrylate) Thin Films Containing Chloroform Molecules, *Solid State Commun.*, 2002, **121**(2–3), p 159–164
12. A. Thander and B. Mallik, Photoinduced Charge-Transfer Between Ferrocene Derivatives and Chloroform Molecules Confined In Poly(Methyl Methacrylate) Thin Films, *Chem. Phys. Lett.*, 2000, **330**(5–6), p 521–527
13. Y. Denga, Y. Sunb, P. Wanga, D. Zhanga, H. Minga, and Q. Zhang, In Situ Synthesis and Nonlinear Optical Properties of Ag Nanocomposite Polymer Films, *Phys. E*, 2008, **40**(4), p 911–914
14. K. Rawlins, A. Lees, S. Fuerniss, and K. Papathomas, Luminescence of $W(CO)_4$(4-Me-phen) in Photosensitive Thin Films: A Molecular Probe of Acrylate Polymerization, *Chem. Mater.*, 1996, **8**(7), p 1540–1544
15. S.C. Farmer and T.E. Patten, Photoluminescent Polymer/Quantum Dot Composite Nanoparticles, *Chem. Mater.*, 2001, **13**(11), p 3920–3926
16. B.J. Ash, D.F. Rogers, C.J. Wiegand, L.S. Schadler, R.W. Siegel, and B.C. Benicewicz, Mechanical Properties of $Al_2O_3$/Poly-methylmethacrylate Nanocomposites, *Polym. Compos.*, 2004, **23**(6), p 1014–1025
17. M. Marinovic-Cincovic, M.C. Popovic, M.M. Novakovic, and J.M. Nedeljkovic, The Influence of β-FeOOH Nanorods on the Thermal Stability of Poly(Methyl Methacrylate), *Polym. Degrad. Stab.*, 2007, **92**(1), p 70–74
18. E. Dzunuzovic, M. Marinovic-Cincovic, K. Jeremic, J. Vukovic, and J.M. Nedeljkovic, Influence of α-$Fe_2O_3$ Nanorods on the Thermal Stability of Poly(Methyl Methacrylate) Synthesized by In Situ Bulk Polymerization of Methyl Methacrylate, *Polym. Degrad. Stab.*, 2008, **93**(1), p 77–83
19. M. Marinovic-Cincovic, Z. Saponjic, V. Djokovic, S. Milonjic, and J.M. Nedeljkovic, The Influence of Hematite Nano-crystals on the Thermal Stability of Polystyrene, *Polym. Degrad. Stab.*, 2006, **91**(2), p 313–316
20. A. Horikawa, K. Yamaguchi, M. Inoue, T. Fujii, and K. Arai, Magneto-optical Effect of Films with Nano-clustered Cobalt Particles Dispersed in PMMA Plastics, *Mater. Sci. Eng. A*, 1996, **217–218**, p 348–352
21. H. Miyazaki, K. Yamauchi, and H. Fukui, Inorganic Fine Particle-Dispersed Pastes with Good Debindering Properties at Low Temperature, Japanese Patent, JP 2008-71983 20080319
22. S.R. Lukić, D.M. Petrović, M.D. Dramićanin, M. Mitrić, and L.J. Đačanin, Optical and Structural Properties of $Zn_2SiO_4$:$Mn^{2+}$ Green Phosphor Nanoparticles Obtained by Polymer Assisted Sol-Gel Method, *Scripta Mater.*, 2008, **58**(8), p 655–658
23. R. Krsmanović, Ž. Antić, I. Zeković, and Miroslav D. Dramićanin, Polymer-Assisted Sol–Gel Synthesis and Characterization of $Zn_2SiO_4$:$Eu^{3+}$ Powders, *J. Alloys Compd.*, 2009, **480**, p 494–498
24. C.C. Klick and J.H. Schulman, On the Luminescence of Divalent Manganese in Solids, *J. Opt. Soc. Am. B*, 1952, **42**(12), p 910–916
25. I.C. Mcneill, A Study of the Thermal Degradation of Methyl Methacrylate Polymers and Copolymers by Thermal Volatilization Analysis, *Eur. Polym. J.*, 1968, **4**(1), p 21–30
26. T. Kashiwagi, A. Inaba, J.E. Brown, K. Hatada, T. Kitayama, and E. Masuda, Effects of Weak Linkages on the Thermal and Oxidative Degradation of Poly(methyl methacrylate), *Macromolecules*, 1986, **19**(8), p 2160–2168
27. I.G. Popovic, L. Katsikas, and H. Weller, The Photopollymerisation of Methacrylic Acid by Colloidal Semiconductors, *Polym. Bull.*, 1994, **32**(5–6), p 597–603
28. L. Katsikas, J.S. Velickovic, H. Weller, and I.G. Popovic, Thermogravimetric Characterisation of Poly(methyl methacrylate) Photopolymerised by Colloidal Cadmium Sulfide, *J. Therm. Anal.*, 1997, **49**(1), p 317–323
29. T. Kashiwagi, T. Hirata, and J.E. Brown, Thermal and Oxidative Degradation of Poly(methyl methacrylate)—Molecular Weight, *Macromolecules*, 1985, **18**(2), p 131–138